An analysis of millimetre-wave interferometry on Hall thruster plumes by finite difference time domain simulations

IOP PUBLISHING JOURNAL OF PHYSICS D: APPLIED PHYSICS

J. Phys. D: Appl. Phys. **41** (2008) 185205 (5pp) doi:10.1088/0022-3727/41/18/185205

An analysis of millimetre-wave interferometry on Hall thruster plumes by finite difference time domain simulations

Jungpyo Lee and Mark A Cappelli

Thermosciences Division, Mechanical Engineering Department, Stanford University, Stanford, CA 94305-3032, USA

Received 4 May 2008, in final form 20 July 2008
Published 28 August 2008
Online at stacks.iop.org/JPhysD/41/185205

Abstract

In this paper, we present finite difference time domain (FDTD) simulations of millimetre-wave propagation through the near-field plasma plume of low power Hall thrusters. The simulations are intended to address potential issues (collisions, magnetic fields) that may affect the validity of simple theory used for phase shift determination in the recent measurements of plasma density using microwave interferometry (Cappelli *et al* 2006 *J. Phys. D: Appl. Phys.* **39** 4582). One-dimensional plane wave FDTD simulations indicate that plasma non-uniformities along the direction of wave propagation have only a minor effect on the phase shifts estimated from collisionless, non-magnetized wave propagation through a path-length averaged plasma slab. Three-dimensional FDTD simulations that also account for electron collisions and magnetic fields indicate that the departure from the use of usual simple models is no more than about 15%, well within the limits of uncertainty in the experimental measurements taken within the near field of these plasma sources.

(Some figures in this article are in colour only in the electronic version)

1. Introduction

Microwave interferometry is a relatively common non-intrusive plasma diagnostic tool originating in the 1960s [1,2] that has recently been used for measuring the electron density in the near [3] and the far field [4] of Hall plasma accelerators. The plasma density is inferred from the measured phase shifts experienced by wave beams transmitted through the plasma, when referenced to the phase of the same source in the absence of the plasma. For plane waves propagating through a uniform, collisionless, non-magnetized plasma slab, theory [5] predicts a rather simple, proportional relation for wave frequency greater than the cut-off (plasma) frequency, between this electron density, n_e, and phase shift, $\Delta\phi$, i.e.

$$n_e = \frac{4\pi m_e \varepsilon_0 c^2}{e^2 \lambda_0 l} \Delta\phi. \quad (1)$$

Here ε_0 is the permittivity of free-space, c the phase velocity of the wave, λ_0 the wavelength, l the length of the path traversed by the wave and e and m_e are the electron charge and mass, respectively.

This result is often applied in non-uniform plasmas, but may not be valid in some applications, where the plasma properties vary strongly in the plane normal and parallel to the direction of beam propagation. Furthermore, it is often applied to both weakly collisional and magnetized plasmas without justification. Modern computational methods, however, provide us with the tools to evaluate the effects of collisions, external magnetic fields and three-dimensional inhomogeneity of plasmas, on the validity of this simple result for specific applications/conditions of interest, particularly those probing the near field of Hall plasma accelerators, where all three factors may contribute to departures from the relationship afforded by equation (1).

In this paper, we report on the results of carrying out a computational analysis using finite difference time domain (FDTD) [6] numerical simulations of the electromagnetic wave propagation to understand the extent to which equation (1) can be faithfully used to interpret recent microwave interferometry data acquired on a low power Hall thruster [3]. FDTD has been used recently to simulate electromagnetic wave propagation through cold, dispersive and magnetized plasmas [7–10]. For our FDTD simulations, we assume the electron density

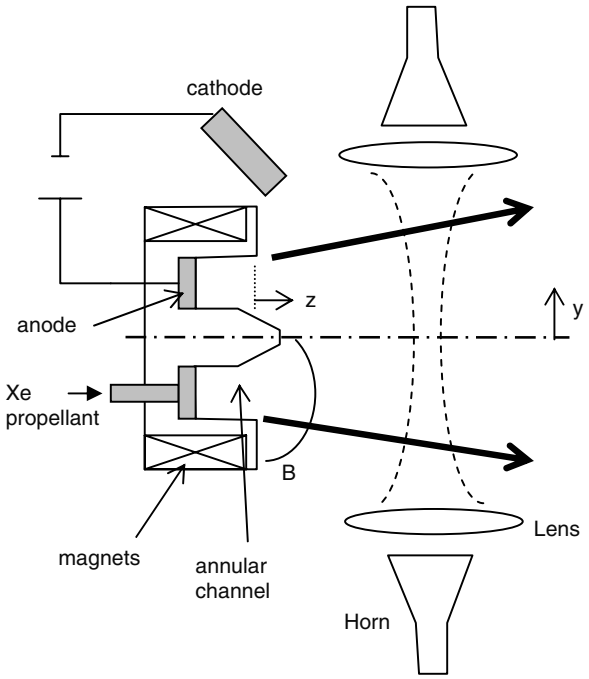

Figure 1. Schematic illustration of microwave interferometry in the near field of a Hall thruster. Note that the x-direction is out of the page (taken from [3]).

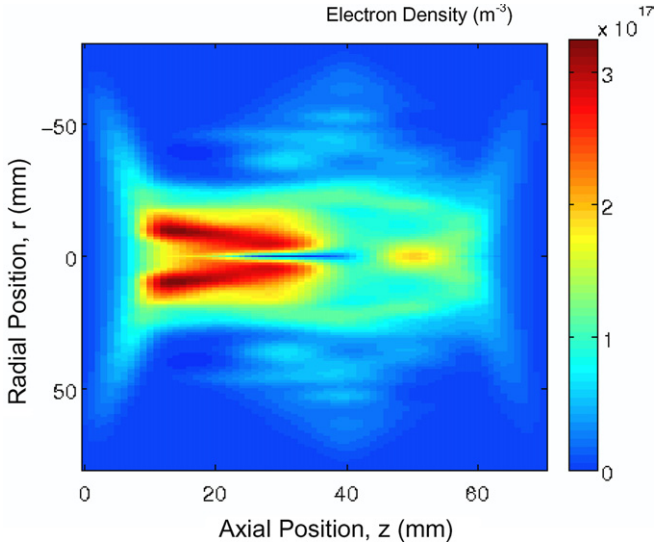

Figure 2. Map of plasma electron density in the near field of a Hall thruster. Note that the channel exit of the thruster is at an axial position $z = 0$ mm.

distribution as measured by Cappelli *et al* [3] from the phase shift data obtained with a 90 GHz phase-bridge interferometer in the near field of a 200 W Hall thruster accelerator. A schematic of the microwave measurements taken from [3] is shown in figure 1. In these measurements, the microwave beam is traversed across various chords passing through the plasma, and the radial variation in the plasma density is reconstructed using the usual onion-peel method, by applying equation (1) to sections of annuli of uniform plasma density along the direction of wave propagation. The inverted plasma density field (n_e variation with radius) is illustrated in figure 2.

In this paper, we compare the FDTD-computed phase shifts resulting from wave propagation through the plasma of figure 2 with those estimated from the use of equation (1). At this time, experimental scatter in the data precludes the application of the inverse problem, i.e. extraction of the plasma density field from the FDTD simulation phase shifts through iterative means until computed phase shifts agree with those measured. The simulations carried out here include collisional effects based on an estimate of the electron–neutral momentum transfer collision frequency and magnetic field. As shown below, while there are differences between the measured and predicted phase shifts on the basis of the assumed plasma density distribution, these differences are found to be within the experimental uncertainty in the electron density measurements.

2. 1D analysis

The governing equations for the electric field ($\boldsymbol{E}$), the magnetic field ($\boldsymbol{H}$) and the electron current density ($\boldsymbol{J}$) for the propagation of an electromagnetic wave in a cold, magnetized plasma are given by Faraday's law, Ampere's law and the balance in the electron momentum [7], i.e.

$$\nabla \times \boldsymbol{E} = -\mu_0 \frac{\partial \boldsymbol{H}}{\partial t}, \tag{2}$$

$$\nabla \times \boldsymbol{H} = \varepsilon_0 \frac{\partial \boldsymbol{E}}{\partial t} + \boldsymbol{J}, \tag{3}$$

$$\frac{\mathrm{d}\boldsymbol{J}}{\mathrm{d}t} + \nu \boldsymbol{J} = \varepsilon_0 \omega_p^2 \boldsymbol{E} + \omega_b \times \boldsymbol{J}. \tag{4}$$

Here, μ_0 is the permeability of free-space, ν the electron collision frequency and $\omega_b = e\boldsymbol{B}_0/m_e$ and $\omega_p = n_e e^2 c/m_e \varepsilon_0$ are the gyro-frequency vector and plasma frequency, respectively, with $\boldsymbol{B}_0$ the external static magnetic field. For the special case of collisionless and non-magnetized plasmas, the assumptions of which are pertinent to the use of equation (1), the collisional drag term, $\nu\boldsymbol{J}$, and the Lorentz force term, $\omega_b \times \boldsymbol{J}$, in equation (4) are neglected. The plasma response to local electric and magnetic fields oscillating at frequency ω results in a plasma permittivity, $\varepsilon_p = \varepsilon_0(1 - (\omega_p^2/\omega^2))$ or the reformulation of Ampere's law as

$$\nabla \times \boldsymbol{H} = \varepsilon_p \frac{\partial \boldsymbol{E}}{\partial t}. \tag{5}$$

As a confirmation of the accuracy of the FDTD analysis, we first applied the FDTD method to the one-dimensional (1D) problem of an electromagnetic plane wave propagating through a non-uniform plasma slab of permittivity $\varepsilon_p = \varepsilon_0(1 - (\omega_p^2/\omega^2))$, and with the electron density variation along the direction of propagation inferred by equation (1) as applied to the measured phase shifts in the experiments of [3]. For the analysis, we represent equations (2) and (5) in the usual finite difference forms in Cartesian coordinate space, with the electric field and magnetic field polarizations along the z and the x-directions, respectively, and plane wave propagation

along y, i.e.

$$H_x\big|_{j+0.5}^{n+0.5} = H_x\big|_{j+0.5}^{n-0.5} - \frac{\Delta t}{\Delta y \times \mu_0}\left(E_z\big|_{j+1}^{n} - E_z\big|_{j}^{n}\right), \quad (6)$$

$$E_z\big|_{j}^{n+1} = E_z\big|_{j}^{n} - \frac{\Delta t}{\Delta y \times \varepsilon_p}\left(H_x\big|_{j+0.5}^{n+0.5} - H_x\big|_{j-0.5}^{n+0.5}\right). \quad (7)$$

Here, n and j represent the indices for temporal and spatial advancement (i.e. along t and y, respectively), Δy is the spatial discretization and Δt the temporal discretization.

The one-dimensional FDTD analysis was carried out several times for propagation along y at various values of x, z (lateral and axial) positions corresponding to the boundary of the plasma domain—represented by an $\frac{80}{\sqrt{2}}$ mm $\times$ $\frac{80}{\sqrt{2}}$ mm square in the x–y plane (perpendicular to the plasma axis). Each calculation uses a distinctive profile for $\varepsilon_p(y)$, i.e. the variation in plasma permittivity along the direction of wave propagation as determined from the spatially varying plasma density (and hence plasma frequency) map shown in figure 2. At the source end of the propagation domain, i.e. at $y = -\frac{80}{\sqrt{2}}$ mm, we initiate the wave with a monochromatic plane wave disturbance at 90 GHz with the electric field polarized in the z-direction. At the other end of the propagation domain, i.e. at $y = +\frac{80}{\sqrt{2}}$ mm, we apply the usual wave absorbing boundary condition to prevent reflection [11]:

$$E_z\big|_{jm}^{n+1} = E_z\big|_{jm-1}^{n} + \frac{c \times \Delta t - \Delta y}{c \times \Delta t + \Delta y}\left(E_z\big|_{jm-1}^{n+1} - E_z\big|_{jm}^{n}\right). \quad (8)$$

Here, jm represents the cell-centre location of the maximum position of the spatial domain in y.

We generally find that the simulations appear to reach a quasi-steady (periodic) state at a propagation distance of $y = \frac{68}{\sqrt{2}}$ mm, where the effects of the upstream presence of an absorbing boundary seemed to be small. For waves at this position, from a time of $t = 0.50$ and 0.60 ns, we obtained the phase shift by Fourier analysis, and reference this to the phase shift obtained by the same simulation for the plane wave propagating in vacuum. The results for the computed phase shifts were found to be weakly dependent on the spatial discretization along the propagation axis. The simulated phase shift at a spacing of five cells per wavelength was found to be about 80% of that simulated for 30 cells per wavelength, with only marginal improvement obtained beyond this grid density. The effect of this spatial discretization seemed to be somewhat independent of the path studied (i.e. for different values of x and z). In all cases, the computational time step was selected to satisfy the stability condition suggested by Taflove and Hagness [6], i.e. $\Delta t \leqslant \Delta y/c$.

In figure 3 we compare the results of the 1D analysis for phase shifts, using the spatial variation in the plasma slab density, to those obtained by the use of equation (1) modified slightly to account for plasma non-uniformities along the path, i.e.

$$\Delta\phi = \frac{e^2\lambda_0}{4\pi m_e \varepsilon_0 c^2}\int_0^l n_e \, dy, \quad (9)$$

Slight differences between the simulated phase shift and that based on the application of equation (9) can be attributed in part to the breakdown of the validity in the use of equation (9), when the path length and region over which the plasma varies substantially are comparable to the wavelength of the electromagnetic wave. This is particularly significant at an axial position of $z = 40$ mm, where the spatial variation in the plasma density seems to be very strong (see figure 2). Despite these limitations, the agreement is seen to be reasonable, confirming in part that the numerical scheme employed is capturing the general behaviour of the wave propagation, and that spatial variations along the direction of the wave propagation do not severely compromise the use of equation (1) for these near-field plasma plume studies.

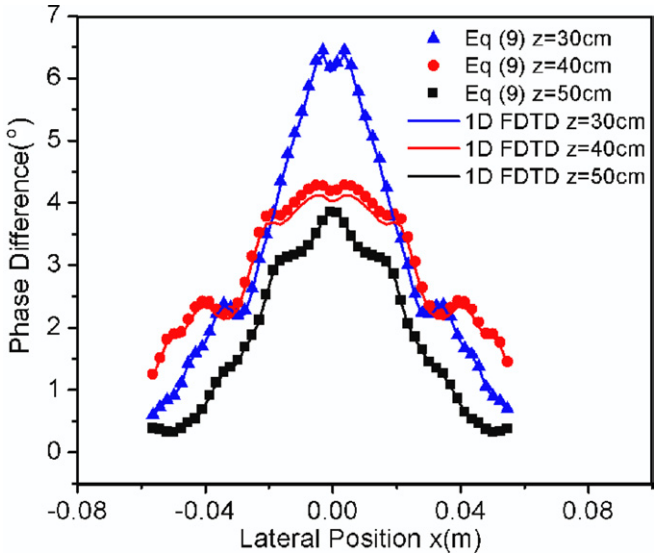

Figure 3. Phase shifts calculated using equation (9) (symbols) and using the 1D FDTD methods (solid lines). The plasma density used for these simulations is that of [3].

3. 3D Analysis

The FDTD analysis was extended to three dimensions (3D), to account for possible plane wave depolarization by the non-uniform plasma dielectric constant. In addition, the 3D analysis was modified to include the effects of electron scattering and electron magnetization due to the presence of a static magnetic field. The analysis applies the 3D finite difference scheme described by Lee *et al* [7] to equations (2)–(4). The electron momentum equation is expressed in explicit matrix form using a Laplace transformation, i.e.

$$\begin{bmatrix} J_x\big|_{i,j,k}^{n+0.5} \\ J_y\big|_{i,j,k}^{n+0.5} \\ J_z\big|_{i,j,k}^{n+0.5} \end{bmatrix} = A(\Delta t)\begin{bmatrix} J_x\big|_{i,j,k}^{n-0.5} \\ J_y\big|_{i,j,k}^{n-0.5} \\ J_z\big|_{i,j,k}^{n-0.5} \end{bmatrix} + \frac{\varepsilon_0}{2}\omega_p^2\big|_{i,j,k}^{n} K(\Delta t)\begin{bmatrix} E_x\big|_{i+0.5,j,k}^{n} + E_x\big|_{i-0.5,j,k}^{n} \\ E_y\big|_{i,j+0.5,k}^{n} + E_y\big|_{i,j-0.5,k}^{n} \\ E_z\big|_{i,j,k+0.5}^{n} + E_z\big|_{i,j,k-0.5}^{n} \end{bmatrix}. \quad (10)$$

In equation (10), i, j and k are the indices for the x, y and z spatial coordinates, and A and K are matrices that define the

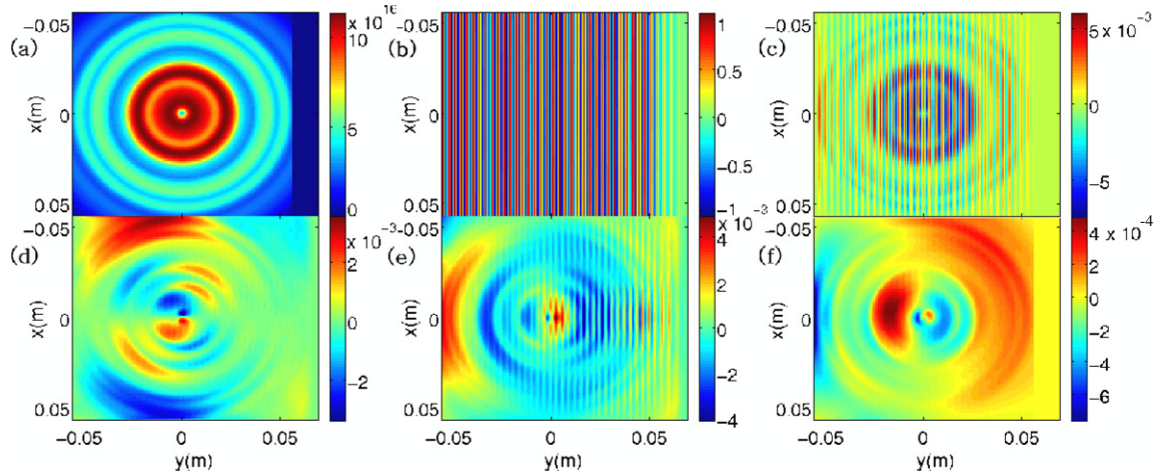

Figure 4. (*a*) The assumed electron density ($n_e(\mathrm{m}^{-3})$), (*b*) the electric field vector in the z-direction ($E_z(\mathrm{V\,m}^{-1})$), (*c*) the induced current density in the z-direction ($J_z(\mathrm{A\,m}^{-2})$), (*d*) the induced electric field vector in the x-direction ($E_x(\mathrm{V\,m}^{-1})$), (*e*) the induced electric field vector in the y-direction ($E_y(\mathrm{V\,m}^{-1})$), (*f*) the induced current density in the y-direction ($J_y(\mathrm{A\,m}^{-2})$) at $z = 40$ mm and $t = 0.5$ ns.

time advancement in the current and electric field, as discussed in detail in [9], which are functions of both ω_b and ν. In this 3D analysis, we specify the components of $\boldsymbol{E}$ and $\boldsymbol{H}$ on the three-dimensional lattice using Yee's algorithm [12], with the components of $\boldsymbol{J}$, ω_b and ω_p located at the cell centre [7].

For the 3D analysis, the domain that the plasma occupied was increased to $\frac{220}{\sqrt{2}}$ mm × $\frac{160}{\sqrt{2}}$ mm × 180 mm in the x, y and z coordinate directions. To minimize spurious reflections from boundaries in this finite computational space, we assigned an extra $\frac{60}{\sqrt{2}}$ mm in the x-direction and 110 mm in the z-direction as redundant space without electrons. An additional 20 cells were added in the y-direction (direction of plane wave propagation) to form a perfect matched layer (PML) with polynomial grading characterized by the absorbance parameters, $m = 3.5$ and $R_0 = 10^{-6}$ [13]. This PML was found to successfully limit reflections at the boundary to less than 10^{-4} times the original amplitude. We also strictly enforce a condition that the component $H_y = 0$ in the y–z plane at the boundaries defined by $x = -\frac{110}{\sqrt{2}}$ mm and $x = \frac{110}{\sqrt{2}}$ mm to prevent wave dispersion along x due to the boundaries.

As in the 1D simulations, plane waves were launched to propagate initially along the y-direction by imposing a sinusoidal variation in E_z on the x–z plane at $y = -\frac{80}{\sqrt{2}}$ mm. We find that the wave achieves a quasi-steady (periodic) state in the x–z plane by 0.5 ns, at a location of $y = \frac{68}{\sqrt{2}}$ mm. As before, phase shifts were calculated from Fourier analysis of the waves between $t = 0.5$ ns and $t = 0.6$ ns. As in the 1D case, we found that the computed phase shifts were weakly sensitive to discretization cell size; we assign an estimated ±5% error due to the finite cell size for all lateral propagations in 3D space. We have carried out a limited set of simulations that indicate that a reduction in cell size beyond 0.2 times the wavelength leads to a gradual increase in the computed phase shift to an asymptotic factor of 1.29. To make the full simulation tractable, we therefore used a rather coarse (equally spaced in x, y and z) grid spacing of five grids per wavelength and corrected the computed phase shift by a factor of 1.29. The stability condition extended to 3D required a time step of $\Delta t \leqslant \Delta y/(\sqrt{3} \times c \times 1.3)$ [6].

The results presented here assume that the initial electron current density, $J_o = 0$ everywhere within the domain, and that the electron collision frequency has an upper value of $\nu = 0.1$ GHz (based on an upper estimate of a background gas density of $10^{20}\,\mathrm{m}^{-3}$, an upper estimate of the electron–xenon momentum transfer collision cross section of $10^{-18}\,\mathrm{cm}^2$ and a mean thermal speed of $10^6\,\mathrm{m\,s}^{-1}$. We used a global value of 1 GHz for the electron gyro-frequency, in accordance with the estimation in [3], aligned along the z-axis. While a uniform collision frequency and electron gyro-frequency is not a true reflection of what is seen in practice in the near field of Hall thrusters, it considerably simplifies the analysis carried out here, and serves mainly to establish the significance of these contributions to the overall phase shifts computed.

Figure 4 provides maps in the x–y plane of the presumed plasma density and the computed components of electric field and induced current density at an axial location $z = 40$ mm. We see that for the cylindrically symmetric electron density (figure 4(*a*)), the wave field component, E_z in figure 4(*b*), induces the electron current along z as shown in figure 4(*c*). Ampere's and Faraday's laws consequently result in the generation of in-plane field components (figures 4(*d*) and (*e*)), as well as current density (e.g. see figure 4(*f*)). The order of magnitude for the induced components E_x and E_y is found to be 10^{-3} times that of E_z when the electron number density is about $10^{17}\,\mathrm{m}^3$.

Figure 5 compares the phase shifts computed by the 3D FDTD analysis to those on the basis of the 1D analysis. The non-uniform plasma distribution in the x–z plane creates a weak variation in E_z in these planes which subsequently affects components of the magnetic field and electron current, causing a distortion in what would otherwise have been a plane wave. The analysis suggests that deviations from 1D plane wave behaviour are strongest very near the discharge exit, between $z = 10$ mm and $z = 30$ mm, where the variation in electron density is relatively severe. Further downstream,

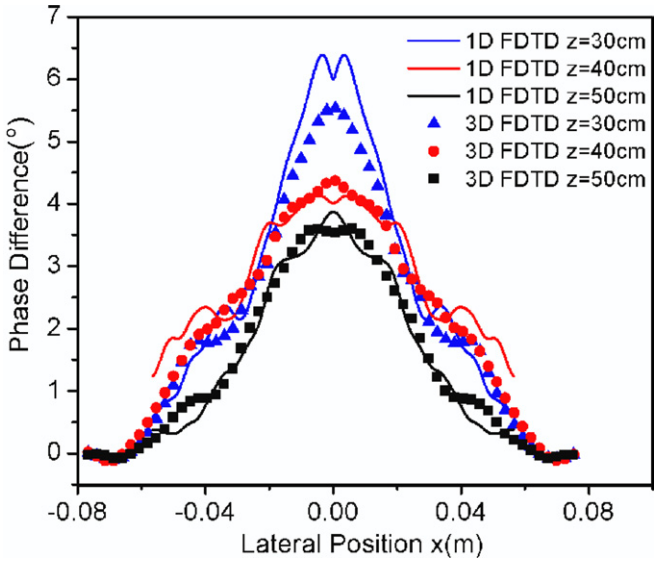

Figure 5. Phase shifts calculated using the 1D (solid lines) and the 3D FDTD methods (symbols). The plasma density used for these simulations is that of [3].

the differences are minor (typically less than 15%) and are certainly within the experimental uncertainty in measured phase shifts, as reported in the experiments of [3]. A sensitivity analysis carried out by varying the electron collision frequency indicates that the weak collisionality of the plasma in the near field of the thruster does not warrant including electron collisions in an interpretation of our interferometer data. In general, we found that the effect of collisions on the phase shift was smaller than -0.2° for values of $\nu \leqslant 0.1\omega$. When the collision frequency was increased to $\nu = 0.5\omega$, we found that the phase shift at $z = 30$ mm was reduced by as much as 1.7°. Also, we find that increases in the gyro-frequency by 10–900% of the nominal value of 1 GHz affected the computed phase shift by a mere $10^{-4\circ}$–0.1°. In extremely low power Hall thrusters, where the near-field magnetic field strength can be much greater than 10^{-2} T, then accounting for the magnetic field may be necessary, however, these lower power thruster plasmas will have scale lengths proportionally smaller, and we expect other effects associated with strong non-uniformities comparable to the wavelength of the microwaves used, to become much more important in the validity of a simple analysis of the measured phase shifts.

4. Summary

FDTD simulations have been performed for millimetre-wave propagation through the near-field plasma plume of low power Hall thrusters. The simulations are intended to address issues such as electron scattering collisions and magnetization that may affect the validity of the use of simple electromagnetic wave propagation theory that is sometimes used for phase shift determination in low pressure magnetized Hall thruster plumes, particularly those recently carried out in the very near field of BHT-200 Hall thrusters [3]. 1D plane wave FDTD simulations indicate that plasma non-uniformities along the direction of wave propagation have only a minor effect on the phase shifts estimated from collisionless, non-magnetized wave propagation through a path-length averaged plasma slab. 3D simulations that account for collisions and electron magnetization indicate that departures from the use of this simple model is no more than about 15%, well within the limits of uncertainty in the experimental measurements taken within the near field of these plasma sources.

References

[1] Heald M A and Wharton C B 1965 *Plasma Diagnostics with Microwaves* (New York: Wiley)
[2] Hermansdorfer H 1968 Microwave diagnostic techniques *Plasma Diagnostics* ed W Lochte-Holtgreven (Amsterdam: North-Holland)
[3] Cappelli M A, Gascon N and Hargus W A Jr 2006 *J. Phys. D: Appl. Phys.* **39** 4582
[4] Gilchrist B E, Ohler S G and Gallimore A D 1997 *Rev. Sci. Instrum.* **68** 1189
[5] Mitchner M and Kruger C H Jr 1973 *Partially Ionized Gases* (New York: Wiley) p 161
[6] Taflove A and Hagness S 2000 *Computation Electrodynamics: The Finite-Difference Time-Domain Method* (Boston, MA: Artech House Publishers)
[7] Lee J H and Kalluri D K 1999 *IEEE Trans. Antennas Propag.* **47** 1146
[8] Kalluri D K, Goteti V R and Sessler A M 1993 *IEEE Trans. Plasma Sci.* **21**70
[9] Kalluri D K and Haung T T 1998 *IEEE Trans. Plasma Sci.* **26** 1022
[10] Kashiwa T, Yoshida N and Fukai I 1988 *IEEE Trans. Antennas Propag.* **36**1096
[11] Mur G 1981 *IEEE Trans. Electromagn. Compat.* **EMC-23** 377
[12] Yee K S 1966 *IEEE Trans. Antennas Propag.* **AP-14** 302
[13] Berenger J P 1994 *J. Comput. Phys.* **114** 185